Applied Mathematics & Information Sciences
An International Journal

http://dx.doi.org/10.12785/amis/091L25

A Hybrid Artificial Intelligence Algorithm for Discrete Optimal Power Flow

*Cong-Hui Huang**

Department of Automation and Control Engineering, Far East University, 74448 Tainan City, Taiwan (R.O.C.)

Received: 26 Nov. 2013, Revised: 27 Mar. 2014, Accepted: 28 Mar. 2014
Published online: 1 Feb. 2015

Abstract: This paper proposes a hybrid immune and simulated annealing algorithm (HISA) to solve equivalent current injection based optimal power flow problem with both continuous and discrete control variables, which is known as discrete optimal power flow (DOPF). Continuous and discrete variables are processed using different techniques; continuous variables (unit active power outputs and generator-bus voltage magnitudes) are solved by current-based OPF, and discrete variable (transformer-tap settings and shunt capacitor devices) using HISA. Computational results indicate that HISA incorporates unique features that include a novel diversity and affinity calculation method, and a redefined crossover and mutation scheme. As a result, HISA performs better in terms of robustness and efficiency in non-convex OPF problems.

Keywords: Equivalent current injection, discrete optimal power flow, immune algorithm, simulated annealing

1 Introduction

The optimal power flow (OPF) problem was first mentioned by Carpentier [1] in 1962 as a network constrained economic dispatch problem. The current-based concept that was proposed to deal with the unbalanced distribution system was extensively tested in [2,3,4]; loads modeled by PQ buses and various formulations could be formed according to network parameters. The handling of non-convex OPF objective functions, along with the unit prohibited operating zones also present problems for mathematical programming of optimal power flow.

In practical power system operation, the OPF problem with both continuous and discrete control variables, taking the valve-point loading effects of the thermal generator into consideration, is a highly constrained, large-dimensional, and non-convex optimization problem [5,6,7]. [8] successfully implemented equivalent current injection (ECI) based hybrid current-power optimal power flow (ECIOPF) with predictor-corrector interior point algorithm (PCIPA). Based on [8], continuous variables could be solved for faster and more accurately.

OPF programs based on mathematical programming have been designed for purely continuous-variable OPF. However, OPF is a mixed-integer non-linear programming (NLP) problem with discrete control variables, such as switchable shunt devices, transformer tap positions, and phase shifters. In the last few decades, several stochastic optimization methods have been developed, such as Genetic Algorithms (GA), Evolutionary Programming (EP), Evolution Strategies (ES), Immune Algorithms (IA), particle swarm optimization (PSO), and Simulated Annealing (SA) [9,10,11,12,13,14]. The application of these algorithms in global optimization problems is desirable because they provide better global search capabilities compared to conventional optimization algorithms. [9] presented a GA-based OPF algorithm for security enhancement that identifies the optimal value of generator active-power output and angle of the phase-shifting transformers. [10] proposed an efficient and reliable EP algorithm with discrete control variables for solving the optimal power flow problem. [12] addressed the short-term unit commitment problem by applying an immune algorithm to power system operation; the IA used an immune memory cell and changed the crossover and mutation ratio from fixed values to the fuzzy system. [13] described the application of a PSO-based OPF method with the individual of continuous control variables structure for solving the OPF problem with the smooth fuel cost of generator.

* Corresponding author e-mail: ch_huang@cc.feu.edu.tw

In this paper, we propose a hybrid immune and simulated annealing algorithm (HISA) for optimal power flow intended for practical applications, which is based on equivalent current-injection with continuous/discrete control variables. This paper is organized as follows: Section 2 formulates the ECIOPF model with PCIPA. Discrete OPF (DOPF) with HISA is discussed in Section 3. Other stochastic search methods are summarized in Section 4, and extensive numerical simulations using the IEEE 30 bus demonstrate that the proposed method is more robust and efficient in comparison. Conclusions are presented in Section 5.

2 Current based OPF problem

The ECIOPF problem can be divided into two parts: 1) the equivalent current injection model and 2) PCIPA for ECIOPF.

2.1 Equivalent current injection model

Figure 1 depicts the π-circuit transmission line model with admittance, $g_{ij} + jb_{ij}$, and shunt line charging susceptance, bc.

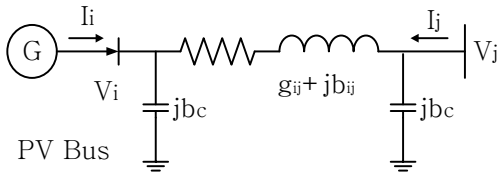

Fig. 1: Transmission line equivalent π model.

According to the Newton-Raphson algorithm, the ECI mismatch equation [3] for the k-th iteration, considering all PQ buses, can be written as:

$$\begin{bmatrix} \Delta I_r^k \\ \Delta I_i^k \end{bmatrix} = \begin{bmatrix} Y_G & -Y_B \\ Y_B & Y_G \end{bmatrix} \begin{bmatrix} \Delta e^k \\ \Delta f^k \end{bmatrix} \tag{1}$$

where the current mismatches are defined by the specified value (spec) minus the calculated (cal) value i.e. $\Delta I = \Delta I_r + j\Delta I_i = I_{spec} - I_{cal}$ and $\Delta V = \Delta e + j\Delta f$ at each iteration. Therefore, the Jacobian for all PQ buses is a state-independent constant matrix.

The injected real power and voltage of PV buses in Figure 1 can be calculated as:

$$P_i = \mathrm{Re}[V_i \times I_i^*] = e_i \cdot I_{i,r} + f_i \cdot I_{i,i} \tag{2}$$

$$|V_i|^2 = e_i^2 + f_i^2 \tag{3}$$

Using Taylor's expansion and substituting from (2) and (3), (1) can be rewritten as:

$$\begin{bmatrix} \Delta P_i^k \\ \Delta |V_i^k|^2 \end{bmatrix} = \begin{bmatrix} \frac{\partial P_i}{\partial e} & \frac{\partial P_i}{\partial f} \\ \frac{\partial |V_i|^2}{\partial e} & \frac{\partial |V_i|^2}{\partial f} \end{bmatrix} \times \begin{bmatrix} \Delta e^k \\ \Delta f^k \end{bmatrix} \tag{4}$$

where

$$\Delta P_i^k = P_i^{spec} - P_i^{cal}$$

$$\Delta \left|V_i^k\right|^2 = \left|V_i^{spec}\right|^2 - \left|V_i^{cal}\right|^2$$

Comparing (4) with (1), the Jacobian has become state-dependent. Jacobian elements with PQ buses do not need to be updated and elements PV buses only need to update some elements in each iteration.

2.2 PCIPA for ECIOPF

In this paper, we formulate the OPF problem as a PCIPA problem [15] where the objective is to minimize the generator cost subject to various constraints. PCIPA is a primal-dual path-following algorithm that solves quadratic and linear formulations, and it is an extension of interior-point. In this study, we discuss a general optimization problem represented as

$$Min \quad F = \left\{ \sum_{i=1}^{ng} (a_i \times P_{Gi}^2 + b_i \times P_{Gi} + c_i) \right\} \tag{5}$$

subject to the conventional load power balance equation in (1) and (4), and the following inequality constraints:

1) *apparent power flow limit of lines*

$$\tilde{S}_{ij} \le \overline{S_{ij}} \text{ and } \tilde{S}_{ji} \le \overline{S_{ji}} \tag{6}$$

2) *bus voltage limits at bus i*

$$\left|\underline{V_i}\right|^2 \le |V_i|^2 \le \left|\overline{V_i}\right|^2 \tag{7}$$

3) *active power generation limits*

$$\underline{P_{Gi}} \le P_{Gi} \le \overline{P_{Gi}} \tag{8}$$

We transform all inequality constraints in the NLP problem model (6)–(8) into equalities by adding non-negative slack vectors ($\mu_i \ge 0$) and the non-negative conditions are handled by incorporating them into logarithmic barrier terms as follows:

$$\begin{aligned} L = & \sum_{i}^{NG} (a_i P_{Gi}^2 + b_i P_{Gi} + c_i) - \lambda^T \begin{bmatrix} I_r^{cal} - I_r^{spec} \\ I_i^{cal} - I_i^{spec} \\ P_G^{cal} - P_G^{spec} - P_{load} \\ \left|V_G^{cal}\right|^2 - \left|V_G^{spec}\right|^2 \end{bmatrix} \\ & - \underline{Z_G^T}(P_G - \underline{\omega_G} - \underline{P_G}) + \overline{Z_G^T}(P_G + \overline{\omega_G} - \overline{P_G}) \\ & - \underline{Z_v^T}(|V|^2 - \underline{\omega_v} - |\underline{V}|^2) + \overline{Z_v^T}(|V|^2 - \overline{\omega_v} - \left|\overline{V}\right|^2) \\ & + \overline{Z_{S,ij}^T}(S_{ij}^2 + \overline{\omega_{S,ij}} - \overline{S_L^2}) + \overline{Z_{S,ji}^T}(S_{ji}^2 + \overline{\omega_{S,ji}} - \overline{S_L^2}) \\ & - \mu \sum_{i=1}^{N} \ln(\underline{\omega_G} + \overline{\omega_G} + \underline{\omega_v} + \overline{\omega_v} + \overline{\omega_{S,ij}} + \overline{\omega_{S,ji}}) \end{aligned} \tag{9}$$

where z represents vectors of Lagrange multipliers, known as dual variables, and $\mu > 0$ is a barrier parameter that monotonically decreases to zero as iterations increase.

Based on the Kaarush-Kuhn-Tucker optimality condition, a set of nonlinear equations can be derived from (9), and the corresponding set of linear correction equations can be derived subsequently by applying Newton's method. The result is the linear correction equation in matrix form.

$$\begin{bmatrix} \nabla_x^2 L & -J_g^T & -J_{\underline{h}}^T & J_{\overline{h}}^T & 0 & 0 \\ -J_g & 0 & 0 & 0 & 0 & 0 \\ -J_{\underline{h}} & 0 & 0 & 0 & I & 0 \\ J_{\overline{h}} & 0 & 0 & 0 & 0 & I \\ 0 & 0 & \underline{W} & 0 & \underline{Z} & 0 \\ 0 & 0 & 0 & \overline{W} & 0 & \overline{Z} \end{bmatrix} \times \begin{bmatrix} \Delta x \\ \Delta \lambda \\ \Delta \underline{z} \\ \Delta \overline{z} \\ \Delta \underline{\omega} \\ \Delta \overline{\omega} \end{bmatrix} = - \begin{bmatrix} \nabla_x L \\ \nabla_\lambda L \\ \nabla_{\underline{z}} L \\ \nabla_{\overline{z}} L \\ \nabla_{\underline{\omega}} L \\ \nabla_{\overline{\omega}} L \end{bmatrix} \quad (10)$$

where $J_g = \nabla_x g(x)$, $J_h = \nabla_x h(x)$ and $\nabla_x^2 L$ can be expressed as

$$\nabla_x^2 L = H_f(x^k) - \sum_{j=1}^{m} \lambda_j^k H_{gj}(x^k) + \sum_{j=1}^{p} (\overline{z}_j^k - \underline{z}_j^k) H_{hj}(x^k) \quad (11)$$

The upper left block of (10) is an augmented Hessian matrix. The elements of a Hessian matrix are the second order partial derivatives of the augmented objective function with respect to all variables. In this paper, PCIPA is executed with a complete augmented gradient vector. Since nonlinear terms are unknown, (10) can be solved by following predictor and corrector steps [16].

3 Application of HISA in DOPF problem

The Hybrid Immune and Simulated Annealing Algorithm, which is described in this paper integrates the Immune Algorithm and Simulated Annealing. In the proposed method, objectives and constraints are first represented as antigen input. This step is followed by antibody production on a feasible space through genetic operations. Genetic operators, such as crossover and mutation through the Redefined Crossover and Mutation Scheme (RCMS), are then processed to produce antibodies in a feasible space. An affinity calculation is also contained within the algorithm and it determines the promotion/suppression of antibody productions. The HISA procedure for the DOPF is described next.

3.1 Initialization and decoding

Antibody initialization with the structural gene chain architecture is performed to generate solution candidates for the DOPF problem. Each gene here indicates a combination of transformer-tap settings and shunt capacitor devices $\pi = [T\ C]$. The population in HISA is represented by an integer matrix of dimension $PS*N$ $(N = N_t + N_c)$, where PS is the population size, and N_t and N_c are the number of transformer-tap settings and shunt capacitor devices, respectively. The antibodies are generated randomly in the feasible space. For the purpose of this study, each gene was between 0 and 20. The genes were decoded as an antibody that was produced by (12). Note that a population pool is composed of these antibodies, and a group of genes forms an antibody.

$$y_i = y_i^{min} + \{\pi_i \times (y_i^{max} - y_i^{min})/step\} \quad (12)$$

where

y_i: the i-th real number of discrete variable
π_i: the i-th gene of discrete variable
$y_i^{\max}$: *the* upper limit of i-th real number
$y_i^{\min}$: the lower limit of i-th real number
Step: sampling number (20 in this study)

3.2 Offspring

Offspring are formed by either the merging of two antibodies from the current generation by a crossover operator or modification of an antibody by a mutation operator. This crossover operator was first proposed by Yamamura, Ono, and Kobayashi [17]. This operator first selects subtours from parents , where subtours contain the common cities. Offspring are created by exchanging subtours, as depicted in Figure 2.

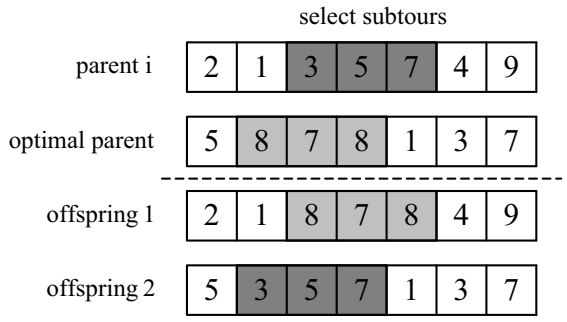

Fig. 2: Example of using the subtour exchange crossover operator.

Mutation is a background operator that produces random changes in various antibodies with a mutation rate equal to Pm. The mutation operator is defined in (13). The mutation operator of HISA is the same as SA, i.e. the optimal parent is always used to form the next offspring. If the offspring is infeasible, another parent will be chosen until a feasible solution is obtained.

$$\pi_i^{offspring} = \pi_i^{optimal} + \gamma \quad (13)$$

where

$\pi_i^{offspring}$: the *i-th* gene of the offspring
$\pi_i^{optimal}$: the *i-th* gene of the optimal parent
γrandom variable between π^{max} and π^{min}

Redefined Crossover and Mutation Scheme (RCMS)

In the sample immune algorithm, crossover generally executes before mutation. A higher crossover rate allows the exploration of the solution space around the parent solution. A high mutation rate explores new solution territory. A lower rate may localize the solution at a local optimum. The offspring lose their resemblance to the parents and the algorithm does not learn from the past and may become unstable. To overcome this, a modified crossover and mutation scheme is proposed as follows:

(i) Generate offspring by introducing *CP(g)* with
(a) if *rand* < *CP(g)*: using crossover
(b) if *rand* > *CP(g)*: using mutation
where
rand: a uniform random number in (0, 1)
CP: the control parameter with initial value set to 0.5, $0 \leq CP \leq 1$
g: the current generation number
In this case, offspring will be generated until all parents have been processed. Since crossover and mutation are both random operators, there is no way of knowing which one is the better of the two. Figure 3 depicts the initial relationship between crossover and mutation in RCMS. The sum of the probability of crossover and mutation equals one.

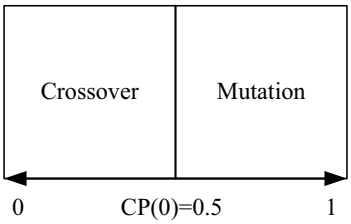

Fig. 3: Initial probability map of crossover and mutation.

(ii) If $F_{best}(g) < F_{best}(g-1)$ are the result of crossover, there is a higher likelihood that the crossover will generate better offspring for the next population. The control parameter will increase as indicated in (14) and the variation of probability of crossover is shown in Figure 4.

$$CP(g+1) = CP(g) + K_1 \tag{14}$$

where
$K_1 = 1/(M * x\_no)$: the regulating factor
M: multiple factor (10 in this paper)
x_no: the number of variables

(iii) If $F_{best}(g) < F_{best}(g-1)$ are the result of mutation, there is higher likelihood for mutation to generate better offspring. The control para- meter will decrease as indicated in (15), and the variation of probability of mutation is illus- trated in Figure 5.

$$CP(g+1) = CP(g) - K_1 \tag{15}$$

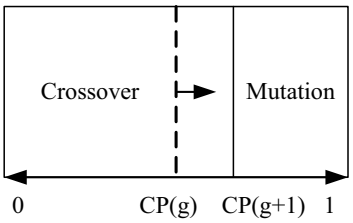

Fig. 4: Variation of probability of crossover.

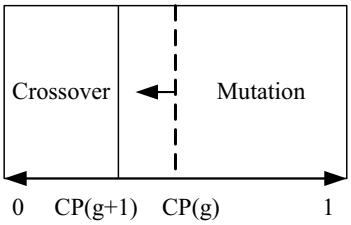

Fig. 5: Variation of probability of mutation.

(iv) If $F_{best}(g) \geq F_{best}(g-1)$, the operation of crossover or mutation needs to hold back.
If it is a result of crossover

$$CP(g+1) = CP(g) - K_2 \tag{16}$$

else if it is the result of mutation

$$CP(g+1) = CP(g) + K_2 \tag{17}$$

and in general, $K_1 < K_2$

3.3 Tabu list

The tabu list is constructed to define forbidden moves, (as in [18])

(i) The solutions just visited except the best solution in the current generation,
(ii) The local optimum is ever visited,
(iii) The antibodies violate the constraints.

3.4 Fitness function evaluation

Each candidate solution is assigned a fitness score to measure its optimality with respect to the objective being optimized. The fitness score of each gene is found by calculating the objective function of ECIOPF. If one or more variables violate their limits, the corresponding antibody will be put into the tabu list to avoid generating the same infeasible solution again.

3.5 Diversity and affinity calculations

HISA produce diverse antibodies by recognizing the affinities between antibodies or between antigens and

antibodies. The quality of solutions in the feasible space can be guaranteed better through the diversity embodiment. To calculate diversity, HISA uses the *Euclidean distance* (*ED*) to substitute for information entropy theory used in IA [19]. AdoptingSA into HISA, the diversity of each antibody is calculated only between the $2*PS$ antibodies (PS parents and PS offspring) and the best antibody. Let the best antibody $y_i(0), i = 1,2,3, \ldots, N$, and $2*PS$ competing antibodies $Y(k) = [y_1(k), y_2(k), \ldots, y_i(k), \ldots, y_N(k)], k = 1,2,3,\ldots,2*PS$, be represented as

$$Y_{best} = [y_1(0)\ \ y_2(0)\ \ \cdots\ \ y_i(0)\ \ \cdots\ \ y_N(0)] \tag{18}$$

The Euclidean distance between the best and competing antibodies is calculated as

$$ED(k) = \sqrt{\sum_{i=1}^{N} [|y_i(0) - y_i(k)|]^2} \tag{19}$$

There are two kinds of affinities under HISA; one elucidates the relationships between two antibodies, where the relative diversity of antibodies, can be evaluated using (20).

$$(Aff_b)^k = (1 + ED(k))^{-1} \tag{20}$$

where $(Aff_b)^k$ is the affinity between the best antibody and the k-th antibody. If all genes in the two antibodies are the same, $ED(k)$ will be zero and the k-th affinity will be one. Therefore, this affinity value lies between zero and one.

The other affinity in HISA is the affinity between the antigen and the antibody, where the combination intensity between the objective and the solution is evaluated as follows:

$$(Aff_g)^k = Obj\_f_k \tag{21}$$

where the Obj_f_k is the value of the objective function with relation to the k-th antibody. The total affinity is calculated from the two affinities as:

$$(Aff)^k = (Aff_g)^k + \alpha \times (Aff_b)^k \tag{22}$$

where α is an adaptive weighting factor calculated as follows:

$$\Delta\alpha = R \times (\alpha_{max} - \alpha_{min})/g \tag{23}$$

$$\alpha(g+1) = \begin{cases} \alpha(g) - \Delta\alpha; & F_{best}(g) \geq F_{best}(g-1) \\ \alpha(g); & F_{best}(g) < F_{best}(g-1) \end{cases} \tag{24}$$

and

$$\alpha(g+1) = \alpha_{min};\ \text{if}\ \alpha(g) - \Delta\alpha < \alpha_{min} \tag{25}$$

where

α_{max}: maximum value of parameter α, set to 0.6
α_{min}: minimum value of parameter α, set to 0.00005
$\Delta\alpha$: the step size
R: the regulating scale, set to 1.05
g: the number of generations

The adaptive weighting factor α is a decreasing parameter similar to the 'temperature' under SA. α depends on the number of generations and the complexity of the system.

3.6 Ranking of selections

Antibodies will be ranked in ascending order according to their total affinity scores by a sorting algorithm. The first PS antibodies are selected and their (Aff)k is used for the next generation. The current best solution (Point A in Figure 6) may not reach the global optimum (Point G), because it is too far. Generally, solutions with slightly better cost (Point B) as calculated by (21) prevail, and so this solution is premature. To prevent premature termination of the algorithm, point G, which has slightly worse cost than B, needs a higher rand value to be selected. That is, a lower (Affb) k is obtained for a longer ED (k). Therefore, the new offspring selected in (20) could prevent premature termination of the algorithm and converge to a global optimal solution.

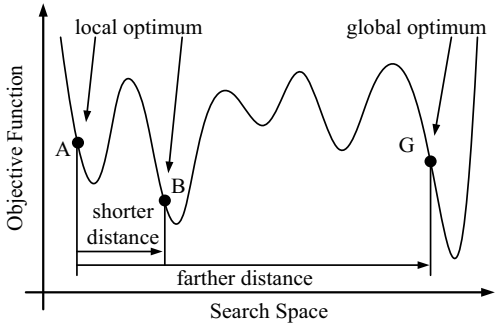

Fig. 6: Visualization of distance.

3.7 Stopping rule

The stopping rule gives the number of iterations reached without improving on the current best solution, and this number is set to 20 for the purpose of this study.

Based on the HISA methodology, an algorithm for solving discrete optimal power flow can be established. The basic flowchart of the algorithm is shown in Figure 7.

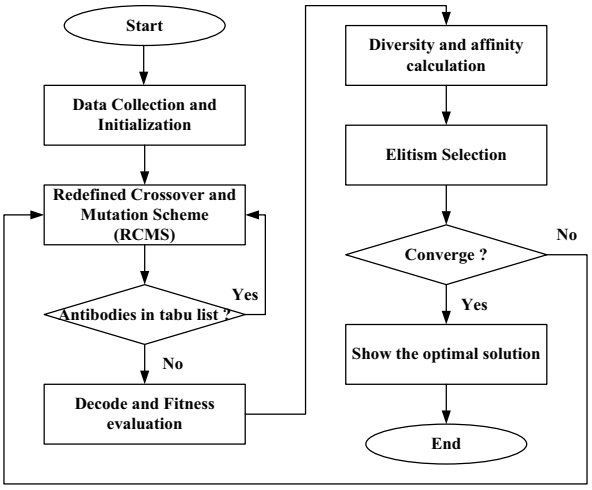

Fig. 7: Flowchart of HISA.

4 Numerical simulation and analysis

The proposed HISA algorithm was tested on a standard IEEE 30-bus test system [20]. The system has 25 control variables, which are as follows: six unit active power outputs, six generator-bus voltage magnitudes, four transformer-tap settings, and nine var-injection values of the shunt capacitor. Three different cases were considered in this study. First, the proposed current-based OPF was applied to obtain the optimal-control variables, which are continuous variables under normal conditions. In the second case, the HISA algorithm was applied to solve the discrete OPF with continuous and discrete variables. In the third case, the proposed HISA algorithm is compared with other AI algorithms, including IA, GA, EP, SA, and ES.

4.1 Optimal solution without discrete variables

In this system, the continuous control variables are the unit active power outputs and generator-bus voltage magnitudes whose limits are listed in [10]. The load demand is 189.2 MW and the objective function is 775.39 \$/h. Convergence tolerance is 10^{-8} for the *barrier parameter* μ, the CPU time is 0.86 seconds, and OPF converges after 9 iterations. The optimal solution with only continuous variables is shown in Table 1, and the values of the objective function for each iteration are shown in Figure 8.

Table 1: The optimal solution of 30-bus system

Unit No.	Bus No.	Unit coefficient a_i	b_i	c_i	V_G [pu]	P_G [MW]	Cost [\$/h]
1	1	0.063	2.5	0.0	1.0049	22.43	87.77
2	2	0.065	2.5	0.0	1.0025	30.77	138.44
3	13	0.040	2.6	0.0	1.1000	40.00	168.00
4	22	0.060	2.4	0.0	1.0145	30.39	128.32
5	23	0.045	2.0	0.0	1.0470	29.15	96.54
6	27	0.040	2.5	0.0	1.0690	38.64	156.32
Total						191.37	775.39

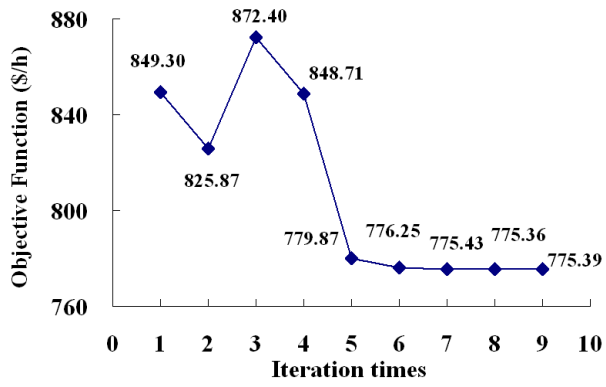

Fig. 8: Objection Function Value Iterations for 30-bus system.

4.2 Optimal solution with HISA

The system has 25 control variables, which are as follows: six unit active power outputs, six generator-bus voltage magnitudes, four transformer-tap settings, and nine var-injection values of shunt capacitor. The unit power output and generator-bus voltage are continuous control variables. The discrete variables are transformer-tap settings and shunt capacitor devices. The adjustable range of the transformer-tap setting is 0.95 p.u. to 1.05 p.u., the step size is 0.005 p.u. The lower and upper limits of the shunt capacitor devices are set from 0.0 to 10 Mvar, respectively, and the step size is 0.5 Mvar. As the optimal solution of the AI problem is different for each run, fifty runs were performed and are examined in Section 4.2 and 4.3.

The optimal solution and the value of discrete variables are shown in Table 2. The operating costs of the best and worst solutions are 772.28 \$/h and 773.94 \$/h (0.21% difference), respectively and the average solution cost is 772.95 \$/h. To show the convergence of HISA, average statistics of the antibody over fifty trials are plotted in Figure 9. The average number of iterations taken to converge and CPU time are 62 times and 1042 s, respectively.

Table 2: Results of IEEE 30-bus system

Generator-bus voltage magnitude, unit real power output and cost							
Unit No.	Bus No.	Best solution VG [pu]	PG [MW]	Cost [\$/h]	Worst solution VG [pu]	PG [MW]	Cost [\$/h]
1	1	1.0328	22.84	89.96	1.0445	22.72	89.31
2	2	1.0306	30.81	138.72	1.0422	30.51	136.77
3	13	1.0897	39.86	167.19	1.1000	40.00	168.00
4	22	1.0201	31.24	133.53	1.0178	30.37	128.22
5	23	1.0569	29.84	99.75	1.0556	29.85	99.78
6	27	1.0671	36.24	143.13	1.0619	37.84	151.86
Total			191.23	772.28	Total	191.28	773.94

Transformer-tap setting				
No.	1	2	3	4
From/To Bus	6–9	6–10	4–12	28–27
Best Tap position	0.965	0.950	0.985	0.965
Worst Tap position	0.950	0.950	0.970	0.955

Bus shunt Admittances									
Shunt No.	1	2	3	4	5	6	7	8	9
Bus No.	10	12	15	17	20	21	23	24	29
Best B_{SH}	1.5	5.0	4.5	4.5	3.5	0.0	6.5	10	0.5
Worst B_{SH}	0.0	2.0	3.0	1.0	3.5	0.5	10	9.5	2.5

4.3 Comparison with other AI algorithms

To ensure a fair comparison, 20 populations were used and 50 test runs were conducted for each method. The

Table 3: Comparison of various methods

Methods		HISA	IA	SA	GA	EP	ES
CPU Time (s)	Min_time(s)	1965	2408	3324	3171	4049	3003
	Max_time(s)	689	239	247	586	894	539
	Avg_time(s)	1042	1114	1602	1555	1916	1549
Cost ($/h)	Worst	773.94	774.46	774.24	773.98	774.00	773.98
	Best	772.28	772.28	772.28	772.28	772.28	772.28
	Average	772.95	773.46	773.45	773.34	773.22	773.47
Count	Max_count	117	151	215	173	249	184
	Min_count	41	15	16	32	55	33
	Avg_count	62.04	69.84	103.62	84.84	117.86	94.9
	PS	20	20	20	20	20	20
	NGO*1	26	12	7	11	13	8
	NGO*2	4	5	8	7	9	5
	NWI	20	20	20	20	20	20

PS: Population size
NGO*1: Number of iterations to reach global optimum(772.28$/h)
NGO*2: Number of iterations to reach sub-optimum(772.72$/h)
NWI: The number of iterations without improving the current best solution

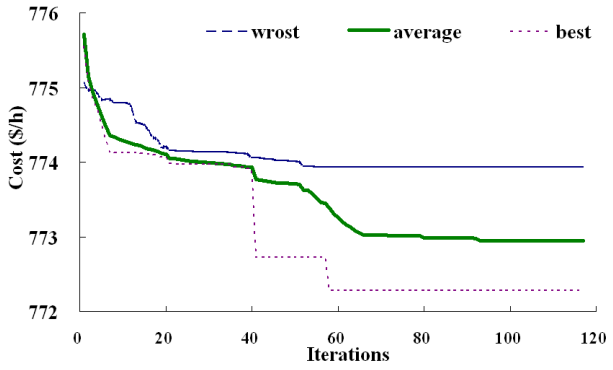

Fig. 9: Convergence of the HISA algorithm.

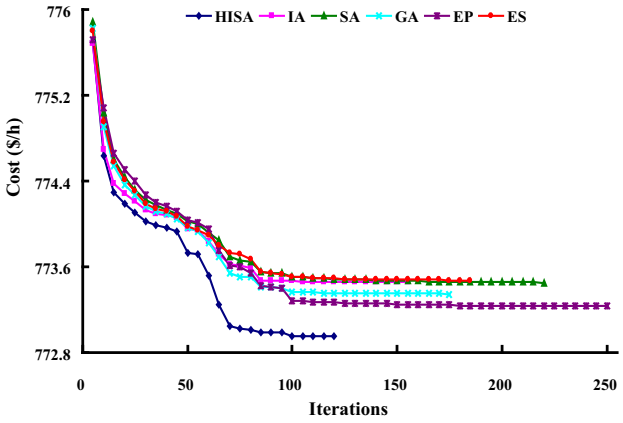

Fig. 10: Convergence comparison.

experimental results are shown in Table 3 including CPU time, unit cost and number of iterations. In addition, the average, maximum, minimum, parameter setting, and the number of iterations taken to reach global and sub-global optimum are also listed. Table 3 shows that every method reaches the optimal solution. However, HISA performs better in terms of the number of generations it takes to converge, the quality of the solution and performance.

Figure 10 depicts the convergence of the average over 50 trials. The HISA method has a steep convergence rate towards an acceptable solution for all cases, thereby demonstrating that the HISA method has a better convergence property than other algorithms tested here.

5 Conclusion

An efficient HISA-based method for solving discrete optimal power flow problems is presented in this study. A novel approach is used to optimize the generator unit cost by using IA and SA algorithms, and for expanding the original IA and SA to the HISA algorithm. The proposed approach searches the local and global neighborhoods to search for optimal cost reduction by adjusting the transformer-tap setting and shunt capacitor. The proposed method performs better than other methods in terms of solution quality, convergence rate and computation efficiency.

The proposed HISA algorithm offers better performance due to the following features:

(1) It integrates the advantages of IA and SA and utilizes a novel estimation of diversity and affinity derived from IA,
(2) It integrates automatic regulation of the frequency of crossover and mutation operations, particularly in applications sensitive to probabilistic rates.

HISA has significant potential for the application of NLP in power system planning and operations.

Acknowledgements

We would like to thank the National Science Council of the Republic of China, Taiwan (Contract No. NSC 100-2221-E-269-018-).

References

[1] J. Carpentiers, Contribution a. 'l'etude du dispatching economique, *Bull. Soc. Francaise Elect.*, **3**, (1962), 431-447.
[2] W. M. Lin, and J. H. Teng, Phase-decoupled load flow method for radial and weakly-mesh distribution networks, *IEE Proc.-Gen. Transm. Distrib.*, **143**, (1996), 39-42.
[3] W. M. Lin, Y. S. Su, H. C. Chin, and J. H. Teng, Three-phase unbalanced distribution power flow solutions with minimum data preparation, *IEEE Trans. on Power Systems*, **14**, (1999), 1178-1183.
[4] W. M. Lin, T. S. Zhan, and M. T. Tsay, Multiple-frequency three-phase load for harmonic analysis, *IEEE Trans. on Power Systems*, **19**, (2004), 897-904.
[5] I. C. da Silva, S. Carneiro, E. J. de Oliveira, J. de Souza Costa, J. L. R. Pereira, and P. A. N. Garcia, A heuristic constructive algorithm for capacitor placement on distribution systems, *IEEE Trans. on Power Systems*, **23**, (2008), 1619-1626.
[6] E. L. Miguelez, F. M. E. Cerezo, and L. R. Rodriguez, On the assignment of voltage control ancillary service of generators in spain, *IEEE Trans. on Power Systems*, **22**, (2007), 367-375.
[7] W. Zhang, F. Li, and L. M. Tolbert, Review of reactive power planning: objectives, constraints, and algorithms, *IEEE Trans. on Power Systems*, **22**, (2007), 2177-2186.
[8] W. M. Lin, C. H. Huang, and T. S. Zhan, A hybrid current-power optimal power flow technique, *IEEE Trans. on Power Systems*, **23**, (2008), 177-185.
[9] D. Devaraj, and B. Yegnanarayana, Genetic-algorithm based optimal power flow for security enhancement, *IEE Proc.-Gener. Transm. Distrib*, **152**, (2005), 899-905.
[10] J. Yuryevich and K. P. Wong, Evolutionary programming based optimal power flow algorithm, *IEEE Trans. on Power Systems*, **14**, (1999), 1245-1250.
[11] G. K. Purushothama, and L. Jenkins, Simulated annealing with local search—a hybrid algorithm for unit commitment, *IEEE Trans. on Power Systems*, **18**, (2003), 273-278.
[12] G. C. Liao, Application of an immune algorithm to the short-term unit commitment problem in power system operation, *IEE Proc.-Gener. Transm. Distrib*, **153**, (2006), 309-320.
[13] M. A. Abido, Optimal power flow using particle swarm optimization, *Electrical Power and Energy Systems*, **24**, (2002), 563-571.
[14] M. R. AlRashidi, and M. E. El-Hawary, Hybrid particle swarm optimization approach for solving the discrete OPF problem considering the valve loading effects, *IEEE Trans. on Power Systems*, **22**, (2007), 2030-2038.
[15] X. Yan and V. H. Quintana, An Efficient Predictor-Corrector Interior Point Algorithm for Security-Constrained Economic Dispatch, *IEEE Trans. on Power Systems*, **12**, (1997), 803-810.
[16] W. M. Lin and S. J. Chen, Predictor-Corrector Interior Point Algorithm for Congestion Relief with FACTS Devices under Deregulation, *Journal of the Chinese Institute of Electrical Engineering*, **19**, (2002), 35-43.
[17] Y. Yamanura, T. Ono, and S. Kobayashi, Character-preserving genetic algorithms for traveling salesman problem, *Journal of Japan Society for Artificial Intelligence*, **6**, (1992), 1049-1059.
[18] W. M. Lin, T. S. Zhan, M. T. Tsay and W. C Hung, The Generation Expansion Planning of the Utility in a Deregulated Environment, *2004 IEEE int. conf. on Electric Utility Deregulation, Restructuring and Power Technologies*, **2**, (2004), 702-707, Hong Kong.
[19] S. J. Huang, An Immune-Based Optimization Method to Capacitor Placement in a Radial Distribution System, *IEEE Trans. on Power Delivery*, **15**, (2000), 744-749.
[20] W. Zhang, F. Li, and L. M. Tolbert, Review of reactive power planning: objectives, constraints, and algorithms, *IEEE Trans. on Power Systems*, **22**, (2007), 2177-2186.

Conghui Huang was born on May 28, 1979. He received his B.S. degree in Electrical Engineering from the National Taiwan University of Science and Technology, Taipei, Taiwan, R.O.C., in 2001 and his M.S. degree in Electrical Engineering and Ph.D. from National Sun Yan-Sen University, Kaohsiung, Taiwan, in 2003 and 2008, respectively. He has been with the Department of Automation and Control Engineering, Far East University, Hsin-Shih, Tainan County, Taiwan, since 2008, where he is currently an Assistant Professor.

His research interests include power systems operation, power systems security, power deregulation, and intelligent solar control systems.